Journal of Sound and Vibration 329 (2010) 84–95

Contents lists available at ScienceDirect

Journal of Sound and Vibration

journal homepage: www.elsevier.com/locate/jsvi

# Efficient prediction of the quality factors of micromechanical resonators

Jinbok Choi [a], Maenghyo Cho [a,*], Jaewook Rhim [b]

[a] WCU Program of Multiscale Mechanical Design, School of Mechanical and Aerospace Engineering, Seoul National University, San56-1, Shillim-dong, Kwanak-gu, Seoul 151-742, Republic of Korea
[b] Agency for Defense Development, Jochiwongil 462, Yuseong, Daejeon, Republic of Korea

ARTICLE INFO

*Article history:*
Received 2 May 2009
Received in revised form
9 September 2009
Accepted 11 September 2009
Handling Editor: L.G. Tham
Available online 8 October 2009

ABSTRACT

A high quality factor (Q-factor) is one of the major requirements of high-performance resonators. An understanding of the dissipation mechanism is crucial for maximizing the quality factor by reducing the energy loss. Thermoelastic damping has been well-known as the important intrinsic dissipation that affects the quality factor of micro-resonators. In this study, a finite element formulation based on the weak form of fully coupled thermoelastic problems is suggested. The coupled thermoelastic equation usually leads to a large-size complex eigenvalue problem, which is very massive and time-consuming to solve. Therefore, we also applied the model order reduction (MOR) scheme to this coupled multiphysical problem in order to achieve computational efficiency. The present approach is validated by comparing the numerical results and analytical solutions.



## 1. Introduction

In recent years, micromechanical resonators have been used in a wide variety of applications, such as gyroscopes, accelerometers, and many other types of sensor. The resonator's quality factor is a key element in the measurement of the performance of micromechanical resonators. It is essential that the resonator vibrate consistently at the desired frequency and that it require as little energy as possible to maintain its vibration. These features can be characterized by the quality factor of the resonator. Generally, the definition of the quality factor is

$$Q = 2\pi \frac{E_{\text{total}}}{\Delta E} = \frac{\omega_0}{2\zeta}, \tag{1}$$

where $E_{\text{total}}$ and $\Delta E$ are the total energy stored and energy dissipated per cycle, respectively. $\omega_0$ is the natural frequency of the system and $\zeta$ is the damping ratio. A higher quality factor indicates a lower dissipation of energy relative to the oscillation frequency. Thus, to obtain a high-performance resonator, the maximization of the quality factor is invaluable. However, the quality factor of the resonator cannot be specified with only one factor. There are various loss mechanisms and the quality factor ($Q$) of the resonator can be expressed in the following form [1]:

$$Q = \left( \frac{1}{Q_{\text{TED}}} + \frac{1}{Q_{\text{anchor}}} + \frac{1}{Q_{\text{fluid}}} + \frac{1}{Q_{\text{surface}}} + \frac{1}{Q_{\text{others}}} \right)^{-1}. \tag{2}$$

* Corresponding author. Tel.: +82 2 880 1693.
*E-mail address:* mhcho@snu.ac.kr (M. Cho).

0022-460X/$ - see front matter © 2009 Published by Elsevier Ltd.
doi:10.1016/j.jsv.2009.09.013

Usually, the devices operate in a vacuum and the contribution of $1/Q_{\text{fluid}}$ is very small and negligible. The most significant mechanism of dissipation in the resonator is thermoelastic damping ($Q_{\text{TED}}$ in Eq. (2)). Thermoelastic damping is a source of intrinsic material damping due to thermoelasticity and arises from the coupling of the strain field with the flow of heat into the material. For instance, the opposite sides of a vibrating beam in the flexural mode experience contrary deformations. When the beam's upper part is compressed, its local temperature increases. The temperature of the lower part of the beam decreases when it is under tension. This phenomenon is repeated continuously while the beam is vibrating in the flexural mode. Thus, the temperature gradients occur locally and irreversible heat-flow is generated due to these temperature gradients. That is, the irreversible heat-flow is the origin of the intrinsic damping.

Zener [2,3] first highlighted the importance of the thermoelastic damping of vibrating structures and suggested analytical expressions for the quality factor of the simple beam model. The theory suggested by Zener is valid for the thin rectangular beam model that vibrates in the flexural mode. The quality factor due to thermoelastic damping is given by

$$Q^{-1} = \frac{E\alpha^2 T_0}{\rho C_p}\frac{\omega\tau}{1+(\omega\tau)^2}, \quad \tau = \frac{b^2}{\pi^2\kappa}, \tag{3}$$

where $E$ is Young's modulus, $\alpha$ is the coefficient of thermal expansion, $T_0$ is the reference temperature, $\rho$ is the density, $\omega$ is the natural frequency and $C_p$ is the specific heat under constant pressure. $\tau$ is the relaxation time that is needed to allow the temperature gradient of the beam to relax, $b$ is the thickness of the beam, and $\kappa$ is the thermal diffusivity($\kappa$=$k/\rho C_p$ ,where $k$ is thermal conductivity).

Lifshitz and Roukes [4] also presented an analytical expression of the quality factor by using the explicitly computed thermal distribution in a beam

$$Q^{-1} = \frac{E\alpha^2 T_0}{\rho C_p}\left(\frac{6}{\xi^2} - \frac{6}{\xi^3}\frac{\sinh\xi+\sin\xi}{\cosh\xi+\cos\xi}\right), \quad \xi = b\sqrt{\frac{\omega}{2\kappa}}. \tag{4}$$

The thermoelastic damping of micro-beam resonators is analyzed through the finite sine Fourier transformation method that is combined with Laplace transformation and the normal mode analysis of Sun et al. [5]. Sun et al. considered the size dependency of thermoelastic damping and various boundary conditions of the beam, which were not considered in the study of Liftshitz and Roukes [4]. However, these expressions work well only for simple beams with rectangular cross-sections and under simple harmonic vibrations in the flexural mode; they are not suitable for structures with complex geometries. By utilizing the perturbation method, Nayfeh and Younis [6] presented an analytical expression for the quality factor of micro-plates of general shapes and boundary conditions under thermoelastic damping. Wong et al. [7,8] considered the application of Zener's theory to thin circular rings and compared their theoretical predictions with experimental results. Recently, an analytical expression for the thermoelastic damping has been also established for axisymmetric out-of-plane vibration of circular plate [9]. Nevertheless, these analytical approaches are limited to relatively simple geometries and boundary conditions. Therefore, a numerical approach, such as the finite-element method, is required for practical applications.

Silver and Peterson [10] proposed a method for predicting thermoelastic damping in beams through the finite element method (FEM). They combined the linear coupled thermoelastic dissipation theory of the beam determined by Zener and the explicit matrix method of Segalman [11]. However, the efficiency of this method has not been verified adequately because the evaluation of the differential stiffness matrix requires the Fourier transform in an integral form, which results in the handling of full matrices in the computation.

A different approach using FEM was presented by Yi [12] to solve the thermoelastic-damping problem. The coupled thermoelastic-damping problem was transformed into an eigenvalue problem by the introduction of the perturbation of displacement and the temperature field. However, in their formulation, unnecessary degrees of freedom (dof) are considered in the velocity, which subsequently increases the total degrees of freedom of the global system matrices. And the computation of thermoelastic damping was also performed by using thermal-energy method in the commercial software ANSYS/Multiphysics [13]. This method has the advantage of significant reduction of computational time because it does not involve complex values and is utilized in commercial package.

In our present work, a finite element for the fundamental equations of thermoelasticity is formulated based on the virtual-work principle. The thermoelastic coupled phenomenon causes the damping and is characterized by a resonance shift [14]. Thus, it is necessary to compute the eigenvalues of the coupled thermoelastic problem to derive the quality factors that are associated with each eigenvalue. The coupled thermoelastic problem induces a quadratic eigenvalue problem (QEP), which is not easy to solve through an iterative eigensolver. Currently, there is no efficient numerical method that can handle the QEP directly. Therefore, the QEP is usually transformed into a generalized eigenvalue problem (GEP) with the same eigenvalues and solved by GEP techniques. However, the GEP requires twice of the degrees of freedom of the original problem. Thus, a lot of computing time and resources are required to compute the complex eigenvalues of practical large size problems, not just for a simple model, such as a beam or plate model. This is one of the crucial issues which have been emerged in a lot of applications of QEPs such as vibration analysis of structural systems, gyroscopic systems, vibro-acoustics and so forth. In the present study, the model order reduction (MOR) method based on Krylov subspaces is adopted to resolve this problem and it proves that the MOR method can be successfully applied to the coupled thermoelastic problem. We can greatly improve the computational efficiency by using the MOR method, which provides us

the same accuracy of natural frequencies in the engineering requirement and quality factors in comparison with the solutions of the original system.

## 2. General thermoelastic theory

The mechanical and thermal behaviors can be represented through the strain and temperature distributions at a specific time. Thus, the state of a structure is specified by reversible heat flow and elastic deformation under the assumption of isothermal conditions. However, the coupling of reversible elastic deformation and irreversible heat transfer due to the heat conduction, which occurs instantaneously, must be considered when the temperature varies over time.

According to the first law of thermodynamics, the energy-conservation relationship can be expressed as follows [15]:

$$\frac{\mathrm{d}}{\mathrm{d}t}(\Pi + K) = L + \frac{\mathrm{d}Q}{\mathrm{d}t}. \tag{5}$$

In Eq. (5), $\Pi$ is the internal energy, $K$ is the kinetic energy, $L$ is the momentum due to the external force, and $Q$ is the heat energy absorbed in the body. The energy terms in Eq. (5) are given as

$$L = \int_V b_i v_i \,\mathrm{d}V + \int_A t_i v_i \,\mathrm{d}A, \quad K = \frac{\rho}{2}\int_V v_i v_i \,\mathrm{d}V, \quad \dot{Q}(=\mathrm{d}Q/\mathrm{d}t) = -\int_A q_i n_i \,\mathrm{d}A + \int_V Q_{\mathrm{gen}} \,\mathrm{d}V \quad \text{and } \Pi = \int_V U \,\mathrm{d}V, \tag{6}$$

where $b_i$ is the body force, $t_i$ is the surface traction, $v_i$ is the velocity vector, and $\rho$ is the density. Further, $q_i$ is the heat-flux vector, $n_i$ is the surface normal vector, $Q_{\mathrm{gen}}$ is the heat energy generated per unit volume and time and $U$ is the internal energy of the body per unit volume. The energy-equilibrium equation is obtained by applying the divergence theorem to Eq. (6)

$$\int_V (\rho v_i \dot{v}_i + \dot{U}) \,\mathrm{d}V = \int_V b_i v_i \,\mathrm{d}V + \int_A t_i v_i \,\mathrm{d}A - \int_V (q_{i,i} - Q_{\mathrm{gen}}) \,\mathrm{d}V. \tag{7}$$

Eq. (7) is rearranged using the relations of the Cauchy formula, $t_i=\sigma_{ij}n_j$, where $\sigma_{ij}$ is the stress tensor, and the divergence theorem, $\int_A t_i v_i \,\mathrm{d}A=\int_A \sigma_{ij} n_j v_i \,\mathrm{d}A=\int_V (\sigma_{ij} v_i)_{,j} \,\mathrm{d}V$. As a result,

$$\int_V [\dot{U} - (\sigma_{ij,j} + b_i - \rho \dot{v}_i) v_i - \sigma_{ij} v_{i,j} + q_{i,i} - Q_{\mathrm{gen}}] \,\mathrm{d}V = 0. \tag{8}$$

From Eq. (8), we can get the following energy-equilibrium equation:

$$\dot{U} = \sigma_{ij}\dot{\varepsilon}_{ij} - q_{i,i} + Q_{\mathrm{gen}} \tag{9}$$

where $\varepsilon_{ij}$ is the strain tensor.

Also, the entropy-balance equation is given by

$$T\dot{S} = -q_{i,i} + Q_{\mathrm{gen}}. \tag{10}$$

Here, $T$ and $S$ represent the temperature and entropy, respectively, and the Helmholtz free energy, ($F(\varepsilon_{ij},T)\equiv U-TS$), is defined and the Taylor-series expansion of the Helmholtz free energy around a prescribed expansion point ($\varepsilon_{ij}=0, T=T_0$) is performed. In this manner, we have the following equation:

$$F(\varepsilon_{ij}, T) = \frac{1}{2} C_{ijkl}\varepsilon_{ij}\varepsilon_{kl} - \beta_{ij}\varepsilon_{ij}\theta - \frac{1}{2} m\theta^2 + \cdots, \tag{11}$$

where $\theta=T-T_0$, $C_{ijkl}=(\partial^2 F(0,T_0))/(\partial\varepsilon_{ij}\partial\varepsilon_{kl})$, $\beta_{ij}=-(\partial^2 F(0,T_0))/(\partial\varepsilon_{ij}\partial T)$, and $m=-(\partial^2 F(0,T_0))/(\partial T^2)$.

If the isotropic properties are considered, Eq. (11) can be expressed as

$$F(\varepsilon_{ij}, T) = \mu\varepsilon_{ij}\varepsilon_{ij} + \frac{1}{2}\lambda\varepsilon_{kk}\varepsilon_{nn} - \gamma\varepsilon_{kk}\theta - \frac{1}{2} m\theta^2, \tag{12}$$

where $\mu$, $\lambda$ are the Lame's constants and the constants, $\gamma$ and $m$, are determined to be

$$\gamma = (3\lambda + 2\mu)\alpha = \frac{E}{1-2\nu}\alpha \text{ and } m = \frac{C_E}{T_0}. \tag{13}$$

Here, $\alpha$ is the thermal expansion coefficient, $\nu$ is Possion's ratio and $C_E$ is the specific heat per unit volume. Therefore, the final form of the Helmholtz free energy is summarized as

$$F(\varepsilon_{ij}, \theta) = \frac{1}{2} C_{ijkl}\varepsilon_{ij}\varepsilon_{kl} - \gamma\varepsilon_{kk}\theta - \frac{C_E}{2T_0}\theta^2, \quad \gamma = \frac{E\alpha_t}{(1-2\nu)}. \tag{14}$$

Then, the following constitutive equations can be derived:

$$\sigma_{ij} = \frac{\partial F}{\partial \varepsilon_{ij}} = C_{ijkl}\varepsilon_{kl} - \gamma\theta, \tag{15}$$

$$S = -\frac{\partial F}{\partial \theta} = \beta_{ij}\varepsilon_{ij} + \frac{C_E}{T_0}\theta = \gamma\varepsilon_{kk} + \frac{C_E}{T_0}\theta = \frac{E\alpha}{(1-2\nu)}\varepsilon_{kk} + \frac{C_E}{T_0}\theta. \tag{16}$$

## 3. Finite element formulations

The weak form of thermoelasticity is derived based on the virtual work principle. To this end, first the displacement and temperature fields are discretized, i.e.,

$$\mathbf{u} = \mathbf{N}_u \mathbf{u}_u \text{ and } \theta = \mathbf{N}_\theta \mathbf{u}_\theta, \tag{17}$$

where $\mathbf{u}$ and $\theta$ are the displacement and temperature fields, respectively. $\mathbf{N}_u$ is the shape function of the displacement field and $\mathbf{N}_\theta$ is the shape function of the temperature field. $\mathbf{u}_u$ and $\mathbf{u}_\theta$ are the displacement and temperature-rise vectors. Therefore, the strain–displacement relationship and the derivative of the thermal field can be represented as

$$\boldsymbol{\varepsilon} = \mathbf{B}_u \mathbf{u}_u \text{ and } \nabla\theta = \mathbf{B}_\theta \mathbf{u}_\theta. \tag{18}$$

Here, $\boldsymbol{\varepsilon}$ is the strain vector and $\mathbf{B}_u$ and $\mathbf{B}_\theta$ are the derivatives of the shape-function matrices of the displacement and temperature-rise, respectively.

The weak form of matrix equations for the thermoelastic problems is derived by considering the variation of the displacement ($\mathbf{u}$) and the temperature rise ($\theta$) with respect to $\delta\mathbf{u}$ and $\delta\theta$. First, we consider the equilibrium equation below

$$\nabla \cdot \boldsymbol{\sigma} + \mathbf{f} = \boldsymbol{\rho}\ddot{\mathbf{u}}. \tag{19}$$

The weak form of the equation is written as follows, by introducing an arbitrary weighting function, $\delta\mathbf{u}$:

$$\int_V \delta\mathbf{u}(\rho\ddot{\mathbf{u}} - \nabla\cdot\boldsymbol{\sigma} - \mathbf{f})\, dV. \tag{20}$$

By integrating the second term by parts and rearranging, we can express Eq. (20) as

$$-\int_V \delta\boldsymbol{\varepsilon}^{\mathrm{T}}\boldsymbol{\sigma}\, \mathrm{d}V + \int_V \delta\mathbf{u}(\mathbf{f} - \rho\ddot{\mathbf{u}})\, \mathrm{d}V + \int_A \delta\mathbf{u}(\boldsymbol{\sigma}\cdot\mathbf{n}^{\mathrm{T}})\, \mathrm{d}A = 0. \tag{21}$$

The local entropy balance equation in Eq. (10) is multiplied by $\delta\theta$ and integrated over the volume

$$\int_V \delta\theta(T_0\dot{S} + \nabla\cdot\mathbf{q})\, \mathrm{d}V = 0. \tag{22}$$

Then, Eq. (22) can be summarized as

$$\int_V \delta\theta T_0\dot{S}\, \mathrm{d}V - \int_V \mathbf{q}\delta(\nabla\theta)\, \mathrm{d}V + \int_A \delta\theta(\mathbf{q}\cdot\mathbf{n})\, \mathrm{d}A = 0. \tag{23}$$

The constitutive equations are given as

$$\boldsymbol{\sigma} = \mathbf{C}\boldsymbol{\varepsilon} - \boldsymbol{\beta}\theta \quad \text{where} \quad \boldsymbol{\beta} = \frac{E\alpha}{1-2\nu}\mathbf{I}, \tag{24}$$

$$\dot{S} = \boldsymbol{\beta}\dot{\boldsymbol{\varepsilon}} + \frac{C_E}{T_0}\theta \tag{25}$$

and

$$\mathbf{q} = -\mathbf{k}\nabla\theta, \tag{26}$$

where Eq. (26) is known as the Fourier's law of heat conduction and $\mathbf{k}(=k\mathbf{I})$ is the thermal conductivity matrix.

By substituting Eqs. (24)–(26) together with Eqs. (17) and (18) into Eqs. (21) and (23), we get

$$\begin{aligned} &T_0\int_V \delta\mathbf{u}_\theta^{\mathrm{T}}\mathbf{N}_\theta^{\mathrm{T}}\boldsymbol{\beta}^{\mathrm{T}}\mathbf{B}_u\dot{\mathbf{u}}_u\, \mathrm{d}V + C_E\int_V \delta\mathbf{u}_\theta^{\mathrm{T}}\mathbf{N}_\theta^{\mathrm{T}}\mathbf{N}_\theta\dot{\mathbf{u}}_\theta\, \mathrm{d}V + \int_V \delta\mathbf{u}_\theta^{\mathrm{T}}\mathbf{B}_\theta^{\mathrm{T}}\mathbf{k}\mathbf{B}_\theta\mathbf{u}_\theta\, \mathrm{d}V + \int_V \delta\mathbf{u}_u^{\mathrm{T}}\mathbf{B}_u^{\mathrm{T}}\mathbf{C}\mathbf{B}_u\mathbf{u}_u\, \mathrm{d}V - \int_V \delta\mathbf{u}_u^{\mathrm{T}}\mathbf{B}_u^{\mathrm{T}}\boldsymbol{\beta}\mathbf{N}_\theta\mathbf{u}_\theta\, \mathrm{d}V \\ &+ \rho\int_V \delta\mathbf{u}_u^{\mathrm{T}}\mathbf{N}_u^{\mathrm{T}}\mathbf{N}_u\ddot{\mathbf{u}}_u\, \mathrm{d}V \\ &= -\delta\mathbf{u}_\theta^{\mathrm{T}}\int_A \mathbf{N}_\theta^{\mathrm{T}}\mathbf{q}\times\mathbf{n}\, \mathrm{d}A + \delta\mathbf{u}_u^{\mathrm{T}}\int_A \mathbf{N}_u^{\mathrm{T}}\mathbf{t}\, \mathrm{d}A + \delta\mathbf{u}_u^{\mathrm{T}}\int_V \mathbf{N}_u^{\mathrm{T}}\mathbf{f}\, \mathrm{d}V \end{aligned} \tag{27}$$

$$\delta\mathbf{u}_\theta^{\mathrm{T}}(\mathbf{C}_{\theta u}\dot{\mathbf{u}}_u + \mathbf{C}_{\theta\theta}\dot{\mathbf{u}}_\theta + \mathbf{K}_{\theta\theta}\mathbf{u}_\theta) + \delta\mathbf{u}_\theta^{\mathrm{T}}(\mathbf{K}_{uu}\mathbf{u}_u - \mathbf{K}_{u\theta}\mathbf{u}_\theta + \mathbf{M}_{uu}\ddot{\mathbf{u}}_u) = -\delta\mathbf{u}_\theta^{\mathrm{T}}\mathbf{F}_\theta + \delta\mathbf{u}_u^{\mathrm{T}}\mathbf{F}_u \tag{28}$$

where $\mathbf{K}_{\theta\theta}=\int_V \mathbf{B}_\theta{}^{\mathrm{T}}\mathbf{k}\mathbf{B}_\theta\, \mathrm{d}V$, $\mathbf{C}_{\theta u}=T_0\int_V \mathbf{N}_\theta{}^{\mathrm{T}}\boldsymbol{\beta}^{\mathrm{T}}\mathbf{B}_u\, \mathrm{d}V$, $\mathbf{C}_{\theta\theta}=C_E\int_V \mathbf{N}_\theta{}^{\mathrm{T}}\mathbf{N}_\theta\, \mathrm{d}V$, and $\mathbf{M}_{\mathbf{uu}}=\int_V \rho\mathbf{N}_u{}^{\mathrm{T}}\mathbf{N}_u\, \mathrm{d}V$, $\mathbf{K}_{uu}=\int_V \mathbf{B}_u{}^{\mathrm{T}}\mathbf{C}\mathbf{B}_u\, \mathrm{d}V$, $\mathbf{K}_{u\theta}=\int_V \mathbf{B}_u{}^{\mathrm{T}}\boldsymbol{\beta}\mathbf{N}_\theta\, \mathrm{d}V$, where $\mathbf{K}_{uu}$ and $\mathbf{K}_{\theta\theta}$ are the stiffness matrices due to the mechanical and thermal fields. $\mathbf{M}_{uu}$ is the mass matrix and $\mathbf{C}_{\theta\theta}$ is the damping matrix due to the thermal field. The matrices, $\mathbf{C}_{\theta u}$ and $\mathbf{K}_{u\theta}$, are respectively, the damping matrix and stiffness matrix due to the thermo-mechanical coupling effect.

From Eq. (28), we obtain the following set of ordinary differential equations:

$$\begin{bmatrix} \mathbf{M}_{uu} & \mathbf{0} \\ \mathbf{0} & \mathbf{0} \end{bmatrix}\begin{Bmatrix} \ddot{\mathbf{u}}_u \\ \ddot{\mathbf{u}}_\theta \end{Bmatrix} + \begin{bmatrix} \mathbf{0} & \mathbf{0} \\ \mathbf{C}_{\theta u} & \mathbf{C}_{\theta\theta} \end{bmatrix}\begin{Bmatrix} \dot{\mathbf{u}}_u \\ \dot{\mathbf{u}}_\theta \end{Bmatrix} + \begin{bmatrix} \mathbf{K}_{uu} & -\mathbf{K}_{u\theta} \\ \mathbf{0} & \mathbf{K}_{\theta\theta} \end{bmatrix}\begin{Bmatrix} \mathbf{u}_u \\ \mathbf{u}_\theta \end{Bmatrix} = \begin{Bmatrix} \mathbf{0} \\ \mathbf{0} \end{Bmatrix}. \tag{29}$$

Here, it is explicitly assumed that the displacement field, ($\mathbf{u}_u$), and the temperature-shift field, ($\mathbf{u}_\theta$), are separable in terms of the position and time

$$\mathbf{u}_u = \hat{\mathbf{u}}_u f(t)\mathbf{u}_\theta = \hat{\mathbf{u}}_\theta f(t), \tag{30}$$

where $f(t)=e^{(i\omega-\delta)t}=e^{\lambda t}$.

The imaginary part, $\omega$, of the complex eigenvalue, $\lambda$, is the natural frequency of vibration and the real part, $\delta$, is the rate of decay of the amplitude. Therefore, the quadratic eigenvalue problem (QEP) is achieved as

$$\{\lambda^2\begin{bmatrix}\mathbf{M}_{uu} & \mathbf{0}\\ \mathbf{0} & \mathbf{0}\end{bmatrix}+\lambda\begin{bmatrix}\mathbf{0} & \mathbf{0}\\ \mathbf{C}_{\theta u} & \mathbf{C}_{\theta\theta}\end{bmatrix}+\begin{bmatrix}\mathbf{K}_{uu} & -\mathbf{K}_{u\theta}\\ \mathbf{0} & \mathbf{K}_{\theta\theta}\end{bmatrix}\}\begin{Bmatrix}\hat{\mathbf{u}}_u\\ \hat{\mathbf{u}}_\theta\end{Bmatrix}=\begin{Bmatrix}\mathbf{0}\\ \mathbf{0}\end{Bmatrix}. \tag{31}$$

The quality factor, $Q$, can be computed as

$$Q=\frac{|\mathrm{Im}(\lambda)|}{2|\mathrm{Re}(\lambda)|}, \tag{32}$$

where $\mathrm{Re}(\lambda)$ and $\mathrm{Im}(\lambda)$ represent the real and imaginary parts of the complex eigenvalues, $\lambda$.

Usually, the methods for solving the quadratic eigenvalue problem, which is given in Eq. (31), can be divided into two categories: one is to treat the problem in its original form and the other is to linearize it into a generalized eigenvalue problem (GEP) of twice the dimension and apply techniques for solving GEPs. The finite element models generally produce large and sparse problems and an iterative solution scheme is the best way of achieving eigensolutions in these cases. However, no effective iterative solver is available for QEP. Of course, a direct method that utilizes the QZ algorithm can be used to get eigensolutions of QEP. However, the computational time is extremely large for a large problem, even though the accuracy of the solution is preserved. Therefore, in this study, the nonlinear QEP is transformed into a linear GEP with the same eigenvalues. Once the eigenvalues of the linear GEP are obtained, the eigenvalues of the QEP can be determined. The most common linearization scheme is the first companion linearization.

For convenience, Eq. (31) is simplified as

$$(\lambda^2\overline{\mathbf{M}}+\lambda\overline{\mathbf{C}}+\overline{\mathbf{K}})\mathbf{x}=\mathbf{0} \tag{33}$$

and the definition, $\mathbf{y}=\lambda\mathbf{x}$, is introduced in Eq. (33). Thus, we can obtain the GEP

$$\left\{\begin{bmatrix}\mathbf{0} & \mathbf{I}\\ -\overline{\mathbf{K}} & -\overline{\mathbf{C}}\end{bmatrix}-\lambda\begin{bmatrix}\mathbf{I} & \mathbf{0}\\ \mathbf{0} & \overline{\mathbf{M}}\end{bmatrix}\right\}\mathbf{q}=\{\mathbf{0}\},\quad \mathbf{q}=\begin{Bmatrix}\mathbf{x}\\ \mathbf{y}\end{Bmatrix}. \tag{34}$$

Thus, it is possible to extract the eigenvalues of the coupled themoelastic damping problem by using an iterative eigensolver that is available for GEPs. Here, it is necessary to note that the matrices $\bar{\mathbf{K}}$,$\bar{\mathbf{C}}$,and $\bar{\mathbf{M}}$ are composed by some submatrices as shown in Eq. (31), whose magnitudes are not in the same order due to physical reasons. This leads to very poor conditions of matrices of the eigenvalue problem in Eq. (34) and, subsequently, yields inaccurate results. Therefore, the governing equations are non-dimensionalized to get all the terms to be closer to one another in magnitude in this study. Stable and reliable numerical results have been obtained through this procedure.

## 4. Reduction of the model for computational efficiency

Of late, a finite element model with large degrees of freedom is often encountered in the field of finite element analysis (FEA) due to the complexity. Such a model requires a lot of computing resources and time. Besides, in our study, the original, second-order dynamics system in Eq. (31) is transformed into the corresponding linear state space system, which has double the dimensions, as shown in Eq. (34). Subsequently, the size of the state space system increases the memory requirements. Therefore, if we can provide an efficient way of replacing the large-scale model with an approximate, smaller model, which is still able to capture the dynamic properties of the original system, we will be able to greatly enhance the computational efficiency. The Krylov subspace method that is based on the moment matching technique has been recognized as one of the desirable ways of model order reduction (MOR) [16,17].

The state-space model can be simplified by appropriately defining the effective stiffness ($\hat{\mathbf{K}}$) and mass ($\hat{\mathbf{M}}$) matrices

$$\{\hat{\mathbf{K}}-\lambda\hat{\mathbf{M}}\}\,\mathbf{q}=\{\mathbf{0}\},\quad \mathbf{q}=\begin{Bmatrix}\mathbf{x}\\ \mathbf{y}\end{Bmatrix},\quad \hat{\mathbf{K}}=\begin{bmatrix}\mathbf{0} & \mathbf{I}\\ -\overline{\mathbf{K}} & -\overline{\mathbf{C}}\end{bmatrix},\quad \hat{\mathbf{M}}=\begin{bmatrix}\mathbf{I} & \mathbf{0}\\ \mathbf{0} & \overline{\mathbf{M}}\end{bmatrix}. \tag{35}$$

The general process of model order reduction is to find an approximated state variable ($\mathbf{z}$) with a small number of degrees of freedom by obtaining the transformation matrix, $\mathbf{T}$, which satisfies the following relation:

$$\mathbf{q}\cong\mathbf{T}\mathbf{z},\ \text{where}\ \mathbf{q}\in\mathbb{R}^N,\mathbf{T}\in\mathbb{R}^{N\times n},\mathbf{z}\in\mathbb{R}^n. \tag{36}$$

Then, we obtain the following, reduced-order system:

$$\{\hat{\mathbf{K}}_r-\lambda\hat{\mathbf{M}}_r\}\mathbf{z}=\{\mathbf{0}\},\quad \mathbf{q}=\mathbf{T}\mathbf{z}, \tag{37}$$

where $\hat{\mathbf{K}}_r=\mathbf{T}^{\mathrm{T}}\hat{\mathbf{K}}\mathbf{T}$ and $\hat{\mathbf{M}}_r=\mathbf{T}^{\mathrm{T}}\hat{\mathbf{M}}\mathbf{T}$.

The stability and accuracy of model order reduction depend on how well the transformation matrix is obtained while preserving the essential properties of the original system.

The reduction is achieved by applying a projection from a higher-order to a lower-order space using the Krylov subspaces that are generated by the Arnoldi algorithm [18]. The $n$th Krylov subspace is defined as

$$K_n(\mathbf{A},\mathbf{b}) = span(\mathbf{b},\mathbf{Ab},\mathbf{A}^2\mathbf{b},\ldots,\mathbf{A}^{n-1}\mathbf{b})\mathbf{A}\in\mathbb{R}^{n\times n},\quad \mathbf{b}\in\mathbb{R}^n : \text{starting vector}. \tag{38}$$

Here, if we set $\mathbf{A}=\hat{\mathbf{K}}^{-1}\hat{\mathbf{M}}$ and $\mathbf{b}=\hat{\mathbf{K}}^{-1}\mathbf{F}$, the $n$th Krylov subspace can be written as

$$K_n(\hat{\mathbf{K}}^{-1}\hat{\mathbf{M}},\hat{\mathbf{K}}^{-1}\mathbf{F}) = span(\hat{\mathbf{K}}^{-1}\mathbf{F},\hat{\mathbf{K}}^{-1}\hat{\mathbf{M}}\hat{\mathbf{K}}^{-1}\mathbf{F},\ldots,(\hat{\mathbf{K}}^{-1}\hat{\mathbf{M}})^{n-1}\hat{\mathbf{K}}^{-1}\mathbf{F}). \tag{39}$$

It is already proved that if the Krylov subspace consists of all linear combinations of the column vectors of the transformation matrix, $\mathbf{T}$, the moments of the reduced system are coincident with those of the original system up to the $n$th order [19].

Therefore, the eigenvalues can be extracted more efficiently by solving the reduced GEP in Eq. (37). The computed eigenvalues of the reduced model agree very well with those of the original model.

## 5. Numerical examples

In this section, some numerical examples are considered to validate the performance and accuracy of the proposed thermoelastic finite element approach and the efficiency of the MOR technique. Thin silicon beams with 30 μm thickness and 30 μm width are taken as the test examples. The material is assumed to be isotropic. Here, we consider two kinds of boundary condition: (i) clamped at both ends of the beam and (ii) a clamped-free condition. The thermal and mechanical properties are given in Table 1. The computational efficiency is also demonstrated through the analysis of resonators with more complex geometries in Section 5.3. The geometries and finite element models are depicted in Figs. 10 and 11, respectively, and their thermomechanical properties are given in Table 6.

The eigenvalue can be obtained by solving the reduced GEP in Eq. (37). First, the desired natural frequency corresponding to a specific vibrational mode (usually, the fundamental mode) is computed through the normal mode analysis without considering the thermal coupling effects. Since the imaginary part of the eigenvalue of Eq. (37) stands for the natural frequency, the natural frequency that is obtained from the normal mode analysis can be an estimate for the complex eigenvalues of the coupled thermoelastic problem.

### 5.1. Clamped–clamped beam resonator

The beam model has been discretized by nine-node quadrilateral elements under the assumption of plane stress. Fig. 1 shows the initial finite element mesh configuration and also represents the deformed shape that corresponds to the fundamental mode of vibration.

The convergence of the quality factor computed by FEM is confirmed when the number of the elements is greater than 40, as shown in Fig. 2. Since we are using higher-order quadrilateral elements, the rate of convergence is relatively faster than when linear finite elements are used [12]. The numerically computed quality factors for the beam with various dimensions are compared with the quality factors that are obtained from the analytical expression suggested by Zener (see Eq. (3)) as represented in Fig. 3. A very good agreement is obtained when the beam is longer than 600 μm. In this example, it is natural to observe a slight difference between the analytical predictions and the present FEM results when the beam is shorter than 600 μm. A discrepancy is observed between the prediction of the present 2-D-plane finite elements and Zener's analytical solution based on the Euler beam theory. In the smaller-length range, the deformation of 2-D plane elements is more flexible and the Euler beam model is constrained by the Euler beam assumption in which no transverse shear deformation is allowed.

The degrees of freedom for this numerical example are increased up to 2138 due to the linearization. Therefore, the required computations are also very time-consuming even though an iterative solver (*eigs*, which is provided by MATLAB) is used. In this study, the model order reduction (MOR) method is adopted, as described in the previous section, to reduce the computational time and memory size. The comparison between the full model and the model reduced through MOR is

**Table 1**
Thermal and mechanical properties of silicon [20].

| Material properties | |
|---|---|
| Thermal conductivity (W/(m K)) | 148 (W/(m K)) |
| Specific heat (J/kg K) | 700 (J/kg K) |
| Coefficient of thermal expansion (1/K) | 2.6e−6 (1/K) |
| Young's modulus ($N/m^2$) | 150e9 ($N/m^2$) |
| Poisson's ratio | 0.2 |
| Density ($kg/m^3$) | 2330 ($kg/m^3$) |
| Reference temperature (K) | 298 (K) |

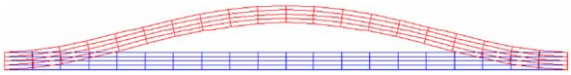

**Fig. 1.** Clamped-clamped beam model with 20 elements along the length and 4 elements across the thickness.

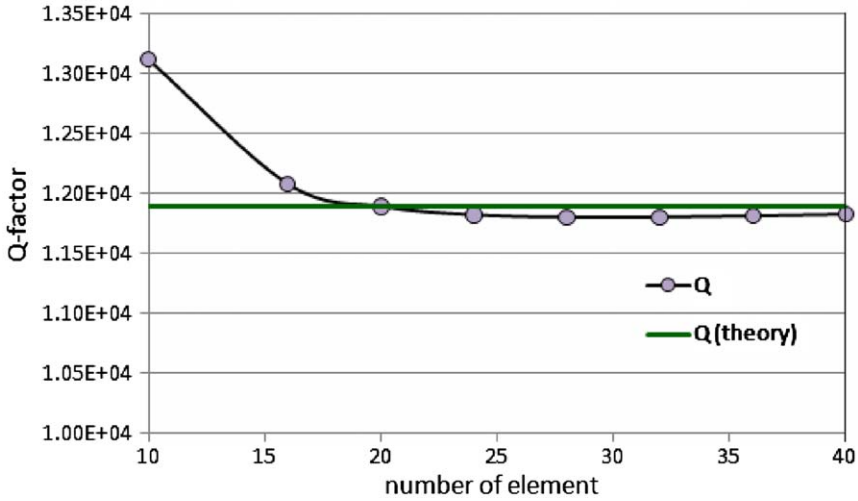


**Fig. 2.** Convergence of numerical solutions (9-node quadrilateral elements).

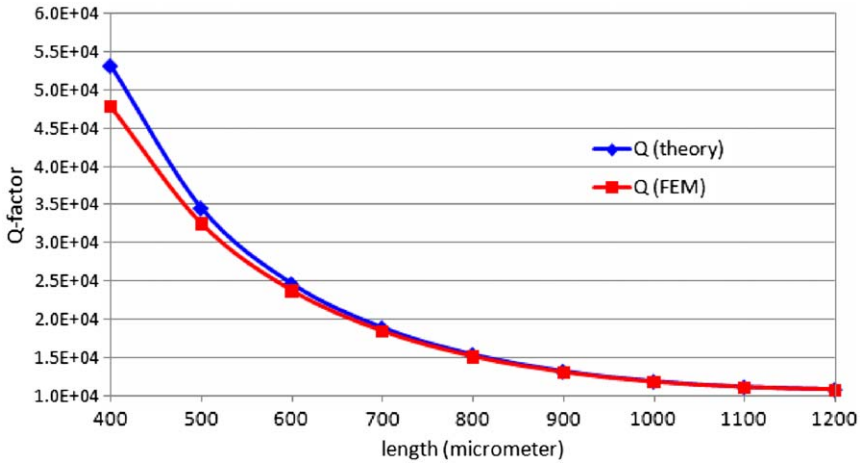


**Fig. 3.** Comparision of the quality factors from Zener's analytical expression and finite-element results (thickness of 30 m).

**Table 2**
Computational time (beam length: 600 μm).

| | FEM (full model) | FEM (MOR) |
|---|---|---|
| DOF | 2138 | 50 |
| Computing time (s) | 1008.5 s | 8.938 s |

summarized in Table 2. For this example, the original model is transformed into the reduced system with 50 degrees of freedom.

However, despite the great reduction in the problem size, the accuracy of the eigensolution is not compromised at all, as shown in Fig. 4. Very good agreement is achieved between the computed quality factors of the original finite element model and those of the reduced model.

In this study, a 3-D thermoelastic element is also developed using 10-node tetrahedral elements. The finite element model and the first bending mode shape are shown in Fig. 5. The test results are summarized in Table 3. A beam with 30 μm

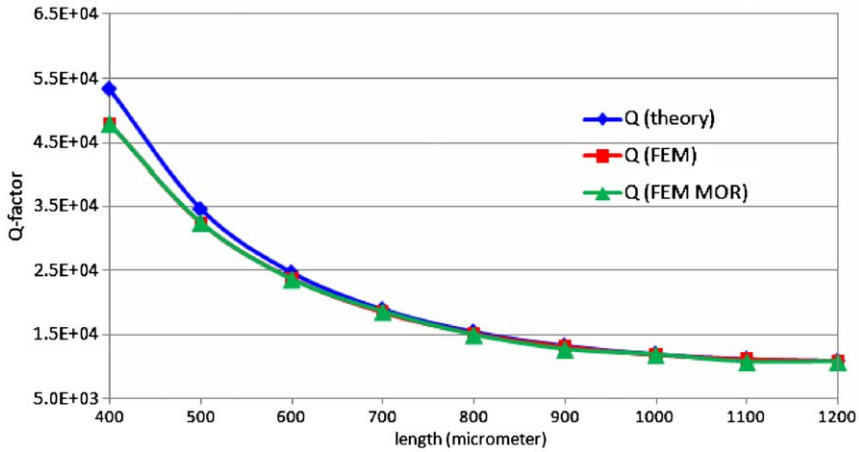


**Fig. 4.** Quality factors obtained from reduction through MOR.

**Fig. 5.** First bending mode of a 3-D micro-beam with both ends clamped.

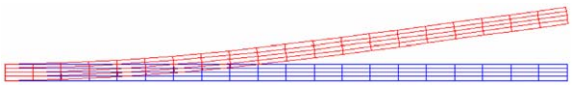

**Fig. 6.** Clamped-free beam model with 20 elements along the length and 4 elements across the thickness.

**Table 3**
Quality factor of a 30 μm × 30 μm × 1000 μm beam that is clamped at both ends.

| Model | DOF | Q-factor | Natural frequency (rad/s) |
|---|---|---|---|
| Zener | | 11,887.449 | 1.55461e6 |
| 9-node quad. | 2138 | 11,828.348 | 1.54886e6 |
| 10-node tetra. | 4960 | 11,656.491 | 1.55333e6 |

width, 30 μm height, and 1000 μm length is prepared for comparison with the above results from 2-D analysis. The finite element mesh is automatically generated in a commercial mesh generator. The number of nodes and elements are 638 and 285, respectively.

As shown in Table 3, in the case of thin-beam problems, the nine-node quadrilateral element yields more accurate results than the 10-node tetrahedral element, even though the degrees of freedom of the former are low. This is because the nine-node quadrilateral element is more flexible than the 10-node tetrahedral element with regard to bending-deformation behaviors.

### 5.2. *Clamped–free beam resonator*

The second example is that of a beam model with different boundary conditions: one side is clamped and the other is free. The initial and deformed mesh configuration corresponding to the first bending mode are illustrated in Fig. 6.

In Fig. 7, the numerical results of the quality factor are compared to the theoretical solutions and the experimental results [21]. An agreement within a 3 percent error-bound is obtained if the aspect ratio is high enough. The model order reduction is also applied to this example; in terms of the quality factor, the results from this approach agree very well with the results for the original system without reduction. Thus, computational efficiency is confirmed (see Fig. 8). In Table 4, there is also a significant reduction in the computational time when the model order reduction (MOR) technique is used, even though the difference in the time is not so large in comparison with the previous example.

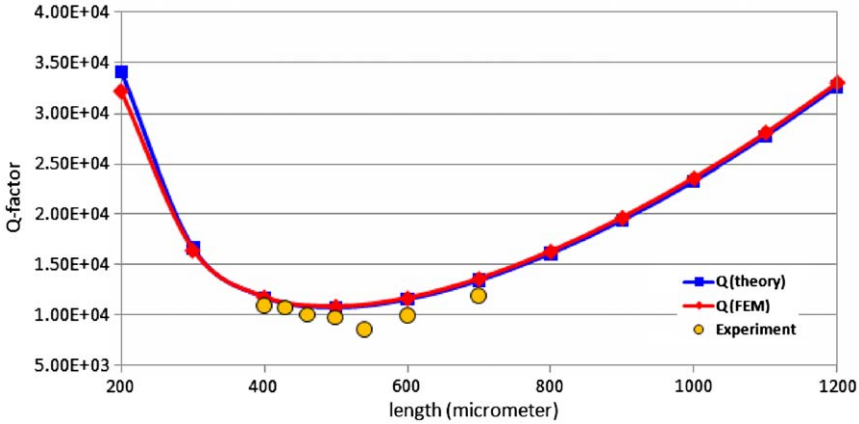


**Fig. 7.** Comparison of quality factors: theory, FEM, and experimental results.

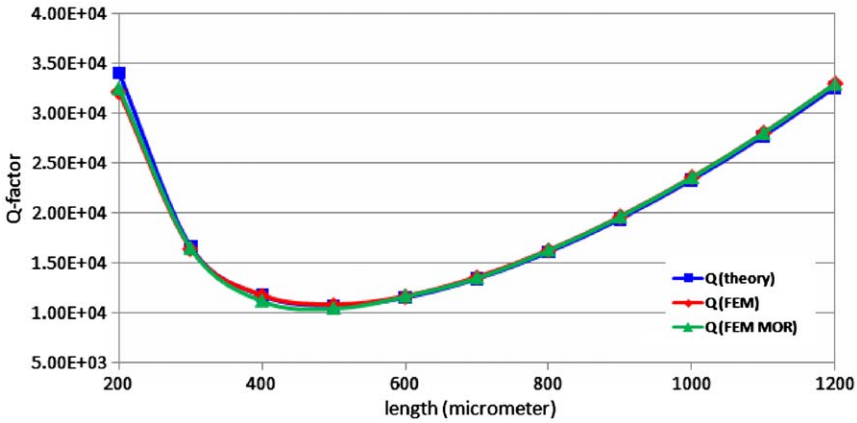


**Fig. 8.** Quality factors through MOR vs. results without MOR.

**Fig. 9.** First bending mode of the 3-D cantilever beam.

**Table 4**
Computational time (beam length: 600 μm).

| | FEM | FEM (MOR) |
|---|---|---|
| DOF | 2176 | 50 |
| Computing time (s) | 94.281 s | 8.234 s |

**Table 5**
Quality factor of a 30 μm × 30 μm × 1000 μm cantilever beam.

| Model | DOF | Q-factor | Natural frequency (rad/s) |
|---|---|---|---|
| Zener | | 23311.954 | 2.44287e5 |
| 9-node quad. | 2176 | 23605.405 | 2.44295e5 |
| 10-node tetra. | 5032 | 23888.720 | 2.44948e5 |

The 3-D finite element model mesh configuration is exactly the same as in the previous example, except for the boundary conditions. The finite element model and the first bending mode shape are shown in Fig. 9. In this numerical example, the accuracy of the 3-D finite element is also a little lower than that of the 2-D plane element; however, an error of less than 3 percent is obtained (see Table 5).

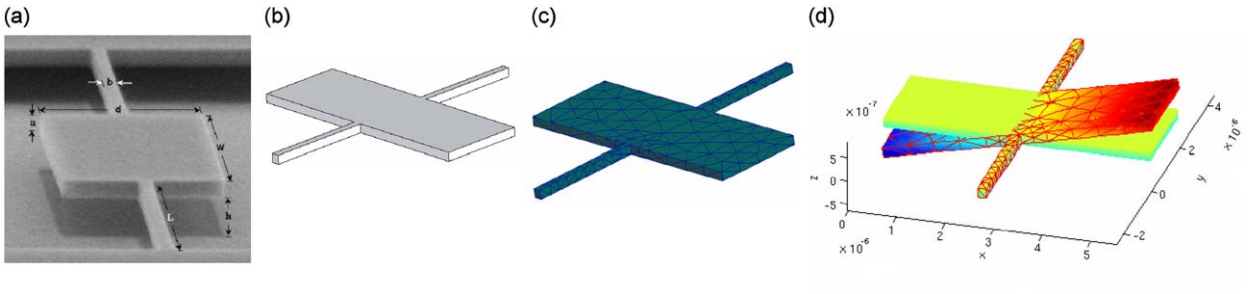


**Fig. 10.** Paddle resonator: (a)SEM image [23] (b) CAD model (c) finite element model (d) fundamental mode shape, both ends of the beam are clamped.

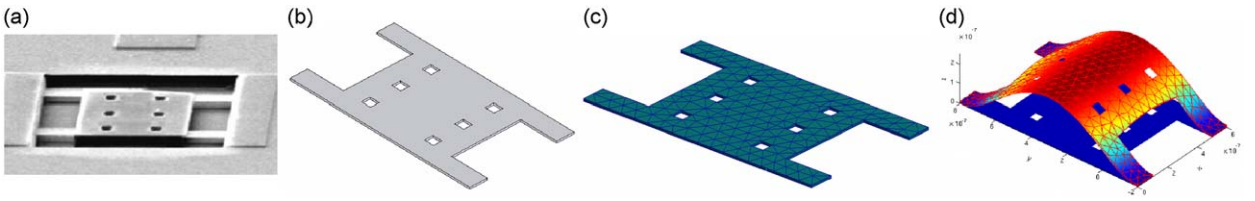


**Fig. 11.** Micromechanical resonator: (a) SEM image [24], (b) CAD model, (c) finite element model and (d) fundamental mode shape.

**Table 6**
Thermomechanical properties.

| Resonator | Paddle resonator [22] | Micromechanical resonator [25] |
|---|---|---|
| Material | Silicon | Aluminum |
| Critical dimensions (μm) | $5.5 \times 2 \times 0.2$ (μm) | $100 \times 60 \times 1$ (μm) |
| Thermal conductivity (W/(m K)) | 130 (W/(m K)) | 237 (W/(m K)) |
| Specific heat (J/(kg K)) | 700 (J/(kg K)) | 898.7 (J/(kg K)) |
| Coefficient of thermal expansion (1/K) | 2.6e−6 (1/K) | 23.6e−6 (1/K) |
| Young's modulus ($N/m^2$) | 180e9 ($N/m^2$) | 70e9 ($N/m^2$) |
| Poisson's ratio | 0.2 | 0.3 |
| Density ($kg/m^3$) | 2330 ($kg/m^3$) | 2679 ($kg/m^3$) |
| Reference temperature (K) | 300 (K) | 300 (K) |

**Table 7**
Natural frequency and quality factor of paddle resonator.

| Simulated Frq. (MHz) | Simulated Frq. [22] (MHz) | Measured Frq. [23] (MHz) | Simulated Q | Simulated Q [22] |
|---|---|---|---|---|
| 4.78 | 4.40 | 5.60 | 2.289e8 | 2.0e8 |

### 5.3. *Paddle resonator and micromechanical resonator with complex geometry*

Two other resonators with more complex geometry are also considered to show the computational efficiency of the suggested method using MOR scheme. Figs. 10 and 11 represent the paddle resonator and micromechanical resonator, respectively. Their thermal and mechanical properties are given in Table 6. Both ends of each beam connected to the paddle are clamped in case of the paddle resonator (Fig. 10). One end of each of the four beams is fixed and the other end is connected to the membrane in case of the micromechanical resonator (Fig. 11). For both numerical examples 10-node tetrahedral elements are used for the convenience of automatic mesh generation.

The computed fundamental natural frequency and corresponding quality factor of the paddle resonator is summarized in Table 7. They are very close to the given data values in the Ref. [22]. As shown in Table 8, the simulated quality factor is larger than the corresponding measured one. This is because the present study considered the thermoelastic damping effect only and neglected all the other environmental energy-loss mechanisms. The significant disagreement between the computed quality factor and measured one has been also reported in Refs. [13,22].

The computational time of each example are given in Table 9. For both examples, the full systems are transformed into the reduced system with 100 degrees of freedom and the significant reduction of computational time can be obtained by

**Table 8**
Natural frequency and quality factor of micromechanical resonator.

| Simulated Frq. (MHz) | Measured Frq. [24] (MHz) | Simulated Q | Measured Q [24] |
|---|---|---|---|
| 40.48 | 39.50 | 6.143e3 | 8.06e2 |

**Table 9**
Computational time comparison.

| | Paddle resonator | | Micromechanical resonator | |
|---|---|---|---|---|
| | FEM | FEM (MOR) | FEM | FEM (MOR) |
| DOF | 9240 | 100 | 16632 | 100 |
| Computational time (min) | N/A | 3.3 | N/A | 10.4 |

utilizing MOR method. For the full systems, the eigenvalue solver (*eigs*) provided by MATLAB [26] did not give the converged eigenvalue and the iteration was terminated after 30 min passed in both cases. So, the full system analysis results in the first colum of Table 9 are not available.

## 6. Conclusions

In this study, a finite element method that considers the fully coupled thermoelastic problem is proposed based on the virtual-work principle. Its performance and accuracy are verified by the solution of micro-beam resonator models for which analytical solutions are available. The computed quality factors obtained by the numerical method are compared to the theoretical and experimental results. The computational efficiency is enhanced by using the Krylov-based model order reduction method (MOR) that reduces the computational time and memory usage without any significant loss of solution accuracy. The suggested numerical approach can overcome the limitations of analytical methods and be applied to practical problems with complex geometries and boundary conditions.

## Acknowledgements

This work was supported by the Defense Acquisition Program Administration and the Agency for Defense Development.

## References

[1] R. Abdolvand, G.K. Ho, A. Erbil, F. Ayazi, Thermoelastic damping in trench-refilled polysilicon resonators, In: Proceedings of 12th International Conference on Solid-State Sensors, Actuators and Microsystems, Boston, June 2005, pp. 324–327.
[2] C. Zener, Internal friction in solids: I. Theory of internal friction in reeds, *Physical Review* 52 (1937) 230–235.
[3] C. Zener, Internal friction in solids: II. General theory of thermoelastic internal friction, *Physical Review* 53 (1938) 90–99.
[4] R. Lifshitz, M.L. Roukes, Thermoelastic damping in micro-and nanomechanical systems, *Physical Review B* 61 (2000) 5600–5609.
[5] Y. Sun, D. Fang, A.K. Soh, Thermoelastic damping in micro-beam resonators, *International Journal of Solids and Structures* 43 (2006) 3213–3229.
[6] A.H. Nayfeh, M.I. Younis, Modeling and simulations of thermoelastic damping in microplates, *Journal of Micromechanics and Microengineering* 14 (2004) 1711–1717.
[7] S.J. Wong, C.H.J. Fox, S. Mcwilliam, Thermoelastic damping of the in-plane vibration of thin silicon rings, *Journal of Sound and Vibration* 293 (2006) 266–285.
[8] S.J. Wong, C.H.J. Fox, S. McWilliam, C.P. Fell, R. Eley, A preliminary investigation of thermo-elastic damping in silicon rings, *Journal of Micromechanics and Microengineering* 14 (2004) 108–113.
[9] Y. Sun, H. Tohmyoh, Thermoelastic damping of the axisymmetric vibration of circular plate resonators, *Journal of Sound and Vibration* 319 (2009) 392–405.
[10] M.J. Silver, L.D. Peterson, Predictive elastothermodynamic damping in finite element models by using a perturbation formulation, *AIAA Journal* 43 (2002) 2646–2653.
[11] D.J. Segalman, Calculation of damping matrices for linearly viscoelastic structures, *Journal of Applied Mechanics and Engineering* 54 (1987) 585–588.
[12] Y.B. Yi, Geometric effects on thermoelastic damping in MEMS resonators, *Journal of Sound and Vibration* 309 (2008) 588–599.
[13] Z. Hao, Y. Xu, S.K. Durgam, A thermal-energy method for calculating thermoelastic damping in micromechanical resonators, *Journal of Sound and Vibration* 322 (2009) 870–882.
[14] J.P. Gorman, Finite element model of thermoelastic damping in MEMS, Master of Science Thesis, Department of Material Science, MIT, 2002.
[15] W. Nowacki, *Thermoelasticity*, second ed., Pergamon Press, Oxford, 1986.
[16] B. Salimbahrami, B. Lohmann, Order reduction of large scale second-order systems using Krylov subspace methods, *Linear Algebra and its Applications* 415 (2006) 385–405.
[17] J.S. Han, E.B. Rudnyi, J.K. Korvink, Efficient optimization of transient dynamic problems in MEMS devices using model order reduction, *Journal of Micromechanics and Microengineering* 15 (2005) 822–832.
[18] R.W. Freund, Krylov-subspace methods for reduced-order modeling in circuit simulation, *Journal of Computational and Applied Mathematics* 123 (2000) 395–421.
[19] T.J. Su, J.R. Craig, Krylov model reduction algorithm for undamped structural dynamics systems, *Journal of Guidance, Control, and Dynamics* 14 (1991) 1311–1313.

[20] R. Ardito, C. Comi, A. Corigliano, A. Frangi, Solid damping in micro electro mechanical systems, *Meccanica* 43 (2008) 419–428.
[21] B.L. Foulgoc, T. Bourouina, O.L. Traon, A. Bosseboeuf, F. Marty, C. Breluzeau, J.P. Grandchamp, S. Masson, Highly decoupled single-crystal silicon resonators: an approach for the intrinsic quality factor, *Journal of Micromechanics and Microengineering* 16 (2006) S45–S53.
[22] A. Duwel, R.N. Candler, T.W. Kenny, M. Varghese, Engineering MEMS resonators with low thermoelastic damping, *IEEE Journal of Microelectromechanical Systems* 15 (2006) 1437–1445.
[23] S. Evoy, A. Olkhovets, L. Sekaric, J.M. Parpia, H.G. Craighead, D.W. Carr, Temperature-dependent internal friction in silicon nanoelectromechanical systems, *Applied Physics Letters* 77 (2000) 2397–2399.
[24] C.L. Dai, C.H. Kuo, M.C. Chiang, Microelectromechanical resonator manufactured using CMOS-MEMS technique, *Microelectronics Journal* 38 (2007) 672–677.
[25] [Online] Available: 〈http://www.memsnet.org/material/〉.
[26] 〈http://www.mathworks.com/〉.